Graph perceiver network for lung tumor and bronchial premalignant lesion stratification from histopathology

Rushin H. Gindra[1,2,3], Yi Zheng[1,4], Emily J. Green[1], Mary E. Reid[5], Sarah A. Mazzilli[1], Daniel T. Merrick[6], Eric J. Burks[7], Vijaya B. Kolachalama[1,4,8,*], Jennifer E. Beane[1,*]

[1]Department of Medicine, Boston University Chobanian & Avedisian School of Medicine, 72 E. Concord Street, Boston, 02118, MA, USA.
[2]Institute of AI for Health, Helmholtz Zentrum Mu¨nchen—German Research Center for Environmental Health, Ingoldstaedter Landstr. 1, Muenchen, 85764, Germany.
[3]Center for Translational Cancer Research (TranslaTUM), School of Medicine, Technische Universitaet Muenchen, Einsteinstraße 25, Muenchen, 81675, Germany.
[4]Department of Computer Science, Boston University, 665 Commonwealth Avenue, Boston, 02215, MA, USA.
[5]Roswell Park Comprehensive Cancer Center, 665 Elm Street, Buffalo, 14203, NY, USA.
[6]Department of Pathology, University of Colorado School of Medicine, 12631 East 17th Avenue, Aurora, 80045, CO, USA.
[7]Department of Pathology & Laboratory Medicine, Boston University Chobanian & Avedisian School of Medicine, 72 E. Concord Street, Boston, 02118, MA, USA.
[8]Faculty of Computing & Data Sciences, Boston University, 665 Commonwealth Avenue, Boston, 02215, MA, USA.

*Contributed equally

Corresponding authors. Vijaya B. Kolachalama & Jennifer E. Beane. Address: 72 E. Concord Street, Boston, 02118, MA, USA. E-mails: vkola@bu.edu; jbeane@bu.edu

Funding

This work was supported by grants from the National Institutes of Health (R21-CA253498, U2C-CA233238, R01-HL159620, R43-DK134273, RF1-AG062109, and P30-AG073104, 1UL1TR001430), Johnson & Johnson Enterprise Innovation, Inc., the American Heart Association (20SFRN35460031), and the Karen Toffler Charitable Trust.

Declaration of Interests

JEB, VBK, SAM, and MER received commercial research grants from Janssen Pharmaceuticals.

Abstract

Bronchial premalignant lesions (PMLs) precede the development of invasive lung squamous carcinoma (LUSC), posing a significant challenge in distinguishing those likely to advance to LUSC from those that might regress without intervention. In this context, we present a novel computational approach, the Graph Perceiver Network (GRAPE-Net), leveraging hematoxylin and eosin (H&E) stained whole slide images (WSIs) to stratify endobronchial biopsies of PMLs across a spectrum from normal to tumor lung tissues. GRAPE-Net outperforms existing frameworks in classification accuracy predicting LUSC, lung adenocarcinoma (LUAD), and non-tumor (normal) lung tissue on The Cancer Genome Atlas (TCGA) and Clinical Proteomic Tumor Analysis Consortium (CPTAC) datasets containing lung resection tissues while efficiently generating pathologist-aligned, class-specific heatmaps. The network was further tested using endobronchial biopsies from two data cohorts, containing normal to carcinoma in situ histology, and it demonstrated a unique capability to differentiate carcinoma in situ lung squamous PMLs based on their progression status to invasive carcinoma. The network may have utility in stratifying PMLs for chemoprevention trials or more aggressive follow-up.

Keywords: Lung cancer, digital pathology, premalignant lesions, deep learning

Introduction

Lung squamous cell carcinoma (LUSC), the second most common type of non-small cell lung cancer (NSCLC), is preceded by the development of bronchial premalignant lesions (PMLs) that can progress toward invasive carcinoma or regress without intervention. Recently, genomic and proteomic profiling of PMLs has demonstrated that PML progression is associated with impaired immunosurveillance[1–5]. Currently, there are ongoing efforts to build a Lung Pre-Cancer Atlas[6] to understand molecular alterations in their spatial context associated with disease severity and progression. To date, H&E-stained tissue slides of PMLs have not been fully utilized as a data source to augment our insights into PML biology. Endobronchial biopsies of PMLs are heterogeneous and contain a range of histologic grades, a variety of structures including cartilage and submucosal glands, and varying degrees of inflammatory cell infiltrate. We hypothesized that computational methods that utilize digitized H&E whole slide images (WSIs) may be able to capture PML heterogeneity and stratify PMLs by histologic severity or their ability to progress to invasive carcinoma, providing a standardized and informative WSI-level assessment of PMLs.

We developed a Graph Perceiver Network (GRAPE-Net) to characterize PMLs using lung tissue WSIs from public cohorts (TCGA[7] and CPTAC[8] consisting of Normal (non-tumor adjacent), lung adenocarcinoma (LUAD) and LUSC tissue samples. GRAPE-Net was trained using TCGA samples and tested using CPTAC samples. It was then used to learn WSI-level features and classes of endobronchial biopsy-based WSIs from two datasets from the University College London (UCL) and the Roswell Park Comprehensive Cancer Institute (Roswell). The network identified signatures that differentiated the lung tissue types, stratified samples by their predominant histologic pattern within LUSC and LUAD tumors and identified carcinoma in situ (CIS) PMLs that progress to LUSC.

Methods

Ethics statement

The Institutional Review Boards at Boston University's Chobanian and Avedisian School of Medicine and the Roswell Park Comprehensive Cancer Center approved the study. All subjects provided written informed consent. Data from TCGA, CPTAC, and UCL are publicly available.

Data acquisition and preprocessing

We obtained digitized H&E images of lung resection tissue and lung tumor subtype annotation from TCGA (534 Normal, 740 LUSC, 808 LUAD) and CPTAC (719 Normal, 685 LUSC, 667 LUAD)[8]. We also obtained the predominant tumor histologic pattern for the CPTAC samples. The endobronchial biopsy-based WSIs were from two datasets: 1) University College London (UCL) (112 CIS samples)[4], defining progression as moving to LUSC; and 2) Roswell Park Comprehensive Cancer Institute (Roswell) (346 samples, normal to CIS spectrum)[1], where progression was persistence of dysplasia or advancement to at least mild dysplasia (**Figure 1a**). The UCL CIS samples included supplementary details about the samples' lymphocyte counts in CIS and stromal regions. The Roswell samples included molecular phenotypes identified using RNA sequencing data such as PML molecular subtype that included 4 categories – proliferative, inflammatory, secretory, and normal-like, as previously described[1].

To evaluate our model's explanations, we selected a few WSIs from CPTAC, Roswell, and UCL and uploaded them to a web-based software (PixelView, deepPath, Boston, MA). Several regions on the WSIs were annotated by board certified thoracic pathologists (D.M. and E.B.) using the software. In the LUAD specimens, tumor areas were annotated by their histologic patterns (solid, micropapillary, cribiform, papillary, acinar, and lepidic). For both LUAD and LUSC tumors, histologic features, including necrosis, lymphatic, and vascular invasions, were also annotated. Airways present in the tissues were graded on the spectrum of normal to CIS and non-tumor tissue areas were labeled as healthy or inflamed lung tissue, stroma, or necrosis. The LUAD and LUSC annotations were combined into tumor, stroma, normal lung, and necrosis for analysis. For the endobronchial biopsy samples, epithelial regions were annotated based on histologic grade (normal, hyperplasia, immature squamous metaplasia, squamous metaplasia, mild dysplasia, moderate dysplasia, severe dysplasia, and CIS). These annotations were combined into CIS, dysplasia, and non-dysplasia for analysis. The overlap between the model-produced heatmaps and the pathologist annotations was analyzed by exporting them as binary images.

WSIs are inherently large, often exceeding dimensions of tens of thousands of pixels in both width and height. This presents challenges for analyzing them due to computational and memory constraints. To address these limitations, each WSI was passed through a fast-patching pipeline at 20x magnification, creating non-overlapping tissue region patches of 256x256 pixels while filtering out background slide information. Key epithelial regions were retained via Otsu thresholding[9]. To prepare the data as input for GRAPE-Net, each WSI was represented as an undirected, unweighted graph with nodes representing the tissue image patches and set of edges connecting the nodes. The graph follows an 8-connectivity

neighborhood structure. The node embeddings in the graph were structured as a matrix of *N* feature vectors, where *N* is the total number of patches in the WSI (nodes in the graph). Each vector is of size 768-dimensions. The features for each patch were obtained from CTransPath[10], a swin-transformer[11] based feature extractor. CTransPath was pre-trained on the TCGA pan-cancer dataset in a self-supervised manner. The graph neighborhood connections are structured as a binary $N \times N$ matrix (adjacency matrix A) with elements $e_{ij} = 1$ if there exists an edge between nodes i and j . These graphs feed into GRAPE-Net, which was then trained for a WSI classification task (**Figure 1b**).

Graph perceiver network

The architectural design of GRAPE-Net consists of three main components (**Figure 2**). (1) A graph convolution block[12] that retains positions information in the input features via edge connections between neighboring nodes, (2) a cross-attention block (PMA) from perceiver[13] which maps variable number of patches per WSI graph to predefined clusters (or "sets"), (3) a self-attention block (SAB)[14] that learns relevant interactions between the sets.

The goal of GRAPE-Net is to learn a representation of the WSI. The graph convolution block contributes to this by stacking multiple graph convolutional layers to learn hierarchical features efficiently. Specifically, the first few layers capture the local, low-level patterns while the deeper layers aggregate them to understand the global structures within the graph. Next, inspired by the recent work on using min-cut pooling on a graph-transformer network (GTP) for WSI level classification[15], and adaptive aggregation functions used in recent graph classification problems[16], GRAPE-Net uses a cross-attention block (PMA) from the perceiver[13]. This module simplifies GTP by replacing the min-cut pooling[17] mechanism with cross-attention layers, which cluster the graph nodes, with similar embeddings and spatial proximity, to predefined latent clusters which we denote as "sets". The number of sets used in the PMA module is a hyperparameter C, typically much smaller than the expected number of visual tokens. The formed sets, accompanied by a classification token CLS, are inputs to the self-attention block, mirroring the approach employed in vision transformers[18]. The SAB assigns weights to each set embedding for classification. The PMA and SAB modules are alternatively stacked, allowing the set embeddings to extract information from the input WSI graph based on the previous layer's learnings. This strategy preserves positional information of the graph nodes in the sets. We followed the weight sharing strategy of the perceiver to optimize computations and reduce memory constraints. The final SAB block is followed by a multi-layer perceptron (MLP), which facilitates multi-class prediction. The CLS token embedding from the SAB represents the slide-level aggregation vector of the weighted sets. The utilization of the CLS token instead of averaging the embeddings of sets facilitates explainability in the network.

Our model introduces novelty by integrating the graph module with the perceiver architecture, enabling sparse graph computations on the visual tokens and computationally efficient modeling of a graph for downstream tasks. For our use-case, it serves as an end-to-end, amortized clustering algorithm, which clusters distinct regions of the tissue into overlapping sets, preserving vital spatial interactions that enhance our comprehension of the biological processes withing tumor tissues.

Experimental design

GRAPE-Net was trained as a three-label classifier (LUAD, LUSC, or Normal). We used the TCGA dataset, with stratified patient-level sampling and 5-fold cross-validation **(Supplementary Figure 1)** with internal testing. The receiver operating characteristic (ROC) and precision-recall (PR) curves for each class were computed along with the accuracy, precision, sensitivity, and specificity as performance metrics (**Figure 1c**). To ensure the classifier is robust to dataset specific batch effects, it was evaluated on the unseen CPTAC cohort. Model weights of the fold with the highest sensitivity (recall) on CPTAC cohort was used for further post-hoc analysis.

To evaluate the effectiveness our proposed network, we compared the model performance with a state-of-the art lung tumor classification model, GTP[15]. Since our model leverages graph convolutions, we also selected a traditional graph classifier, Graph Isomorphism Network (GIN)[12] for comparison. To ensure fair comparison, we used CTransPath[10] as the common feature extractor for all methods and used the same cross-validation parameters for training. The hyper-parameters stated in the respective published research of GTP and GIN were used to achieve the best performance on TCGA and CPTAC cohorts. Optimal hyperparameters for our network configuration involved a hidden dimension (D) of 64, a graph block with 3 GINConv layers, a cross-attention pooling configuration of 200 sets and a 3 self-attention layers per self-attention block (SAB). We used 8 heads for multi-head attention training. To avoid overfitting, we used dropouts with a rate of 0.2 in feed-forward blocks, and binary cross-entropy loss to enhance robustness. Training was completed over 30 epochs in 8-sample mini-batches, using early stopping, a 0.0003 initial learning rate, a step scheduler, and the Adam optimizer[19] for expedited convergence. All the experiments were performed on a single GeForce RTX 2080Ti 11Gb workstation.

For post-hoc analysis, the WSI-level features for each sample were extracted by giving the respective graphs as input to the trained 3-label GRAPE-Net classifier. The 64-dimensional features from the final layer of the network were considered as the representations for each WSI and used for further analysis. UMAP manifold representations[20]and principal component analysis (PCA) representations were plotted to illustrate the relationship between image features and sample phenotypes (**Figure 1c**). Sample phenotypes were grouped as follows: normal adjacent lung tissue, LUSC, and LUAD for the lung tissue data (CPTAC). Within CPTAC, we examined differences in the principal components associated with LUSC predominant histologic patterns (keratinizing or non-keratinizing) and LUAD predominant histologic patterns grouped as follows: (solid/micropapillary/cribriform or lepidic/acinar/papillary). Within the CIS samples, we examined differences in the principal components by progression status. Post-hoc analysis results suggest that the model is robust to cohort-based batch effects between Roswell and UCL cohorts.

Explainability analysis

GRAPE-Net learns the classification label-relevant contributions of the tissue regions during training. We show these explanations as heatmaps using a relevance propagation mechanism[21](**Figure 1c**). This mechanism is a generic attention-based model explanations

for bimodal transformers. It uses attentions and gradients from the SAB and PMA blocks to produce relevancy maps for each interaction between the sets *C* and the assigned nodes *N*. The relevancy map from PMA provides the individual contributions of each node (patch) for the final prediction instead of distributing the contribution of each set as an average to all the nodes within the set. These relevancy maps are constructed on the WSI using the adjacency matrix A and coordinates of all the patches on the WSI.

Statistical analysis

We compared the performance of GRAPE-Net with other approaches for the tumor classification task in lung cancer (train on TCGA-Lung, test on CPTAC-Lung) highlighting its efficiency while performing like the state-of-the-art methods. UMAP and PCA clustering analyses were conducted using Scanpy framework [22]. Clustering performance was evaluated using adjusted Rand score and adjusted mutual index with higher scores displaying good clustering for user-specified labels. Statistical significance between principal components and sample characteristics were assessed through two-tailed t-tests and Spearman's correlation coefficient experiments with analyses performed at a significance $p = 0.05$.

Data availability

Data from TCGA and CPTAC can be downloaded freely from the public domain. UCL data can be obtained from: https://idr.openmicroscopy.org with IDR0082. Roswell images can be accessed via the Human Tumor Atlas Network Data Portal (https://humantumoratlas.org/) using the file identifications provided in **Supplementary Table 1**.

Code availability

Computer scripts and manuals are made available on GitHub (https://github.com/vkola-lab/ajpa2024).

Results

GRAPE-Net Performance

GRAPE-Net demonstrated high classification performance on TCGA (mean AUROC=0.98 ± 0.01 & mean AUPRC=0.98 ± 0.01) and CPTAC data (mean AUROC=0.93 ± 0.01 & mean AUPRC=0.95 ± 0.02) **(Figure 3)**, utilizing significantly fewer resources compared to two published frameworks (**Table 1**), *GRAPE-Net* ~ 202K vs *GTP* ~ 664K trainable parameters). Five-fold cross validation indicated good agreement between the true and predicted tumor classes on both the TCGA and CPTAC data, across different folds displaying the robustness of the model to data bias used for training and testing. For each sample, three separate class activation maps were produced to highlight the areas of normal and tumor tissue (LUAD or LUSC) in each WSI. The generated class-specific heatmaps were consistent with the expert pathologist annotations from 20 CPTAC samples (selected at random), accurately pinpointing areas corresponding to same-label annotations (**Figure 4a** and **Supplementary Figure 3).** These results illustrate that GRAPE-Net can distinguish between the NSCLC tumor subtypes and the normal tissue regions within a WSI, and therefore, we wanted to further explore its ability to detect subtle distinction between tumor histologic patterns and PML histology.

Stratification of Tissues by Morphologic Features

We hypothesized that GRAPE-Net could differentiate between predominant histologic patterns of LUSC and LUAD tumors and lung squamous PML histology by discerning subtle morphological features. To test this, we used the WSI latent features from the CPTAC, UCL, and Roswell samples to perform UMAP-based clustering (**Figure 5**). Clustering segregated normal, LUAD, and LUSC with a high adjusted Rand score of 0.69 and adjusted mutual information score of 0.64. Principal component analysis (PCA) on the latent features (**Supplementary Figure 2**) revealed significant PC1 differences between keratinizing and non-keratinizing LUSC tumors (PC1: $p = 0.01$), with the latter PC2 values like those of LUAD tumors. The LUAD tumors showed significant PC1 differences between aggressive (solid/micropapillary) and non-aggressive (lepidic/acinar/papillary) histologic patterns (PC1: $p = 5.4e\text{-}14$). Notably, LUAD (solid/micropapillary) tumors exhibited PC2 values similar to LUSC tumors, as solid LUAD tumors require immunohistochemical analysis for diagnosis as they can be difficult to distinguish from LUSC tumors.[23]

UMAP and PCA revealed most endobronchial biopsies were proximal to the normal cluster, with some high-grade dysplasia and CIS PMLs clustering with LUAD and LUSC cases ($p < 0.01$ for PML vs. LUAD, PML vs. LUSC, on both PC1 and PC2). Roswell biopsies did not show significant separation by histology, molecular subtype, or progression status (**Supplementary Figure 2c**).

All CIS samples from Roswell and some from UCL grouped with LUSC tumor cases (75% of CIS samples were classified as LUSC tumors with $p < 0.01$ for CIS vs. LUAD, CIS vs. LUSC on both PC1 and PC2). Among the UCL biopsies with progression status to LUSC, the model robustly stratified regressive versus progressive CIS. GRAPE-Net performance predicting regressive CIS as Normals (pNORMAL) and Progressive CIS as Tumors (pLUSC) was as follows: Precision = 0.68, Recall = 0.67, Specificity = 0.38, Accuracy = 0.67, and AUC=0.69

(**Table 2**). Additionally, in prior work on the UCL dataset[4], an automated deep learning pipeline was used to quantify the density of lymphocytes, epithelial cells, and stromal cells in the CIS and stromal regions. The study showed a significant decrease in lymphocyte density (p=0.02) and increase in epithelial cell density (p=0.005) in CIS regions in progressive versus regressive samples. Using GRAPE-Net, we observed a similar significant decrease in lymphocyte density (p=1.03e-6) and an increase in epithelial cell density (p=1.4e-4) between CIS samples predicted as Tumors (pLUSC) versus Normals (pNORMAL). Spearman correlation between the PC values and the respective CIS region lymphocyte and epithelial cell densities suggested that PC1 has a high positive correlation and PC2 has a high negative correlation with epithelial density. PC2 is also positively correlated with lymphocyte density (**Table 2**). Both PC1 and PC2 are significantly different between CIS progressive versus regressive lesions (p=0.005 and p=1.1e-5, respectively). These results suggest that the model learns certain morphological characteristics pertaining to CIS progression status highlighted using relevance heatmaps as shown in **Figure 4b** and Supplementary **Figure 4.**

Discussion

In this work, we introduce the Graph Perceiver Network (GRAPE-Net) that is designed to stratify bronchial PMLs which are precursors to invasive LUSC. The goal was to distinguish PMLs with a high likelihood of progressing to LUSC from those that may regress without intervention. Utilizing H&E stained WSIs, GRAPE-Net stratifies PMLs across a continuum from normal to tumor tissues. Using four distinct datasets, the model generated latent features observable across sample types (resected lung tissue versus endobronchial biopsies) that were associated with tumor histologic patterns and CIS PMLs progression status to invasive carcinoma.

GRAPE-Net's performance was demonstrated through its high classification accuracy on TCGA and CPTAC lung resection tissue datasets, coupled with its efficient generation of pathologist-aligned, class-specific heatmaps. Principal component analysis (PCA) on the WSI latent features demonstrated separation within LUAD and LUSC samples based on predominant histologic pattern. On the endobronchial biopsy WSIs, GRAPE-Net identified CIS lesions that progressed to LUSC. The principal components of the latent features were associated with decreases and increases in lymphocyte and epithelial cell densities within CIS regions, respectively, in progressing versus regressing lesions. GRAPE-Net's predictive capacity on CIS lesions may have clinical utility in prioritizing patients for chemoprevention trials or by potentially shortening screening intervals via bronchoscopy.

Our framework currently does not differentiate between biopsies with and without bronchial dysplasia, likely due to a paucity of training data on the cellular morphology changes characteristic of various dysplasia stages (i.e., mild, moderate, and severe). This limitation underscores the necessity for future research to expand model training with a broader array of bronchial PMLs. Additionally, it will be important to test our model on lung adenomatous premalignant lesions (including atypic adenomatous hyperplasia and adenocarcinoma in situ) as biopsies of these lesions become available via robotic bronchoscopy. Looking forward, we advocate for the assessment of GRAPE-Net across more extensive cohorts and

the integration of additional bulk, single cell, and spatial resolved molecular data into the model to refine PML stratification.

Acknowledgment
We would like to thank Ms. Erin Kane for coordinating the upload of the Roswell slides to the Human Tumor Atlas Network public data portal.

Author Contributions
Study conception (JEB, VBK); method development (RHG, YZ, VBK, JEB); interpretation of results (RHG, VBK, JEB, EJB); pathologic annotation (EJB, DTM, EJG); sample acquisition and clinical data curation (MER, SAM, JEB); writing of the manuscript (RHG, VBK, JEB).

Table 1: Performance metrics for the 3-label (Normal vs LUAD vs LUSC) classification task. Mean performance metrics(%) with standard deviation values in parentheses are reported for the GRAPE-Net method used in this study and two other previously published state of the art methods in the TCGA and CPTAC datasets.

		Precision			Recall/Sensitivity			Specificity			Accuracy
Method	Data	Normal	LUAD	LUSC	Normal	LUAD	LUSC	Normal	LUAD	LUSC	All
GRAPE-Net	TCGA	97.6(0.8)	89.7(2.1)	88.7(2.6)	99.0(0.5)	88.8(2.1)	88.8(2.2)	99.1(0.3)	93.5(1.3	93.8(1.0)	91.4(1.0)
	CPTAC	95.9(2.2)	79.7(3.2)	88.8(2.7)	95.3(2.0)	89.6(3.6)	78.1(5.1)	97.8(1.3)	89.0(2.4)	95.0(1.5)	87.8(1.1
GTP[15]	TCGA	96.0(1.5)	90.5(2.3)	90.7(1.9)	98.5(1.0)	89.8(1.5)	89.7(1.6)	98.6(0.6)	94.0(1.4)	94.9(0.8)	92.0(1.2)
	CPTAC	92.8(7.5)	82.9(4.5)	91.1(4.3)	96.9(1.7)	88.9(5.0)	78.5(7.4)	95.5(5.3)	91.0(3.3)	95.9(2.6)	88.2(2.1)
GIN[12]	TCGA	97.3(1.2)	89.7(2.5)	85.7(3.6)	98.4(1.1)	85.9(3.3)	89.2(2.8)	99.0(0.4)	93.8(1.6)	92.1(1.4)	90.3(1.7)
	CPTAC	95.9(0.2)	82.5(0.4)	78.3(0.3)	89.0(6.8)	83.5(3.5)	82.8(4.4)	97.9(1.2)	91.5(2.3)	88.5(2.4)	85.2(1.6)

Table 2: Significance statistics for comparing model feature space with sample characteristics for CIS premalignant lesions. To demonstrate GRAPE-Net's ability to stratify PMLs, we show the model's classification performance predicting regressive CIS as Normals (pNORMAL) and Progressive CIS as Tumors (pLUSC)**.** Additional test statistics were also done with other metadata characteristics, with p-value<0.05 considered significant. Significant scores highlighted in **bold.**

Test Description	Test Statistic	P-Value (<0.05)
T Tests		
Lymphocyte Density in CIS regions (pLUSC v pNORMAL)	**-5.18**	**1.03e-06**
Epithelial Density in CIS regions (pLUSC v pNORMAL)	**3.94**	**0.000145**
PC1 (Progression v Regression)	**2.82**	**0.005721**
PC2 (Progression v Regression)	**-4.59**	**1.18e-05**
Spearman Correlation Coefficient		
Lymphocyte Density in CIS regions v PC1	-0.099	0.2932
Lymphocyte Density in CIS regions v PC2	**0.297**	**0.0024**
Epithelial Density in CIS regions v PC1	**0.506**	**0.0002**
Epithelial Density in CIS regions v PC2	**-0.749**	**0.0002**
Classification Metrics		
Precision	0.68	-
Recall	0.67	-
Specificity	0.38	-
Accuracy	0.67	-
AUC	0.69	-

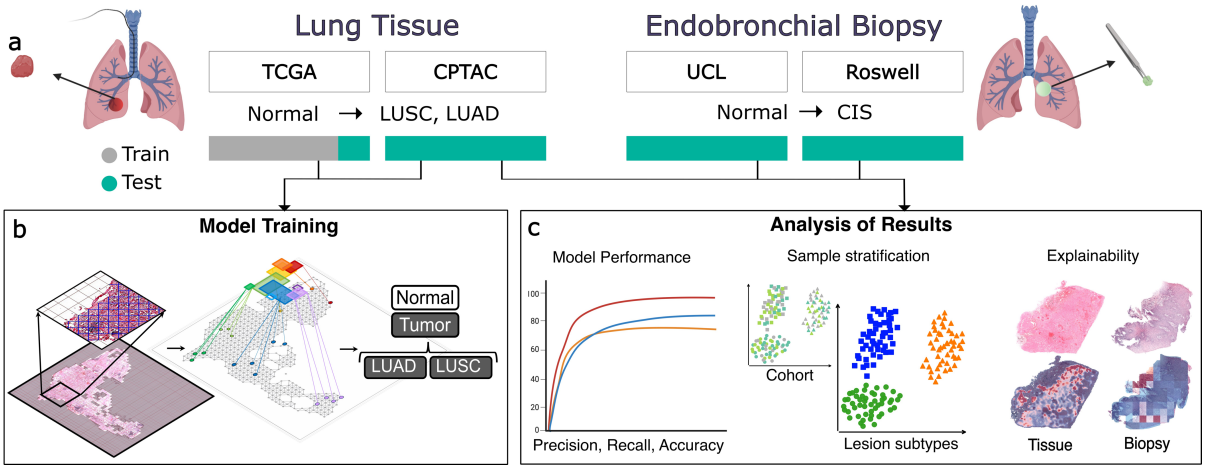

Figure 1: Overview of the study. **(a)** Digitized H&E-stained images were obtained from 4 different datasets including lung resection tissues (TCGA and CPTAC datasets) with normal tissue adjacent to the tumor (Normal), lung adenocarcinoma (LUAD), and lung squamous cell carcinoma (LUSC) and endobronchial biopsies (UCL and ROSWELL datasets) ranging from normal to carcinoma in situ (CIS) histology. The model was trained on TCGA data and test across TCGA, CPTAC, UCL, and ROSWELL datasets. **(b)** Graph Perceiver Network (GRAPE-Net) overview trained to differentiate lung cancer subtypes. **(c)** Overview of analysis conducted using the results of the model that included evaluation of model performance, WSI features with clustering-based metrics, and model explainability using class-specific heatmaps.

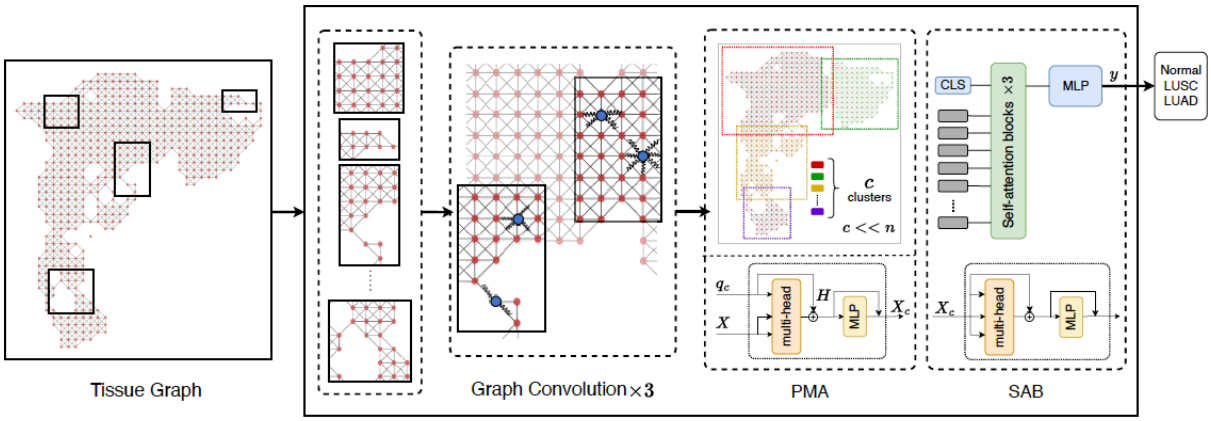

Figure 2: Graph perceiver network (GRAPE-Net) architecture. Each whole slide image (WSI) is represented as an undirected, unweighted tissue graph, where each node is an embedding of features in an image patch. Our proposed GRAPE-Net aggregates neighborhood information via graph convolutions while preserving spatial context[12]. To efficiently find the neighborhood interaction between the different tissue regions in the tumor

micro-environment, the graph is clustered to 'C' overlapping sets by pooling the nodes using multi-head cross-attention block (PMA). The fixed set embeddings are then given as input to the self-attention block (SAB), which learn morphologic interactions with its neighborhood and relevance of each set towards the specific output label of interest. The aggregated attentions are then given as input to a multi-layer perceptron (MLP) for classification of the WSI as either Normal, LUAD or LUSC. Here, the layer-specific feature representation of the graph is denoted as H. A CLS (or class) token is added to serve as the entire WSI representation, which is used for classification and computing the relevance of each graph node towards the prediction.

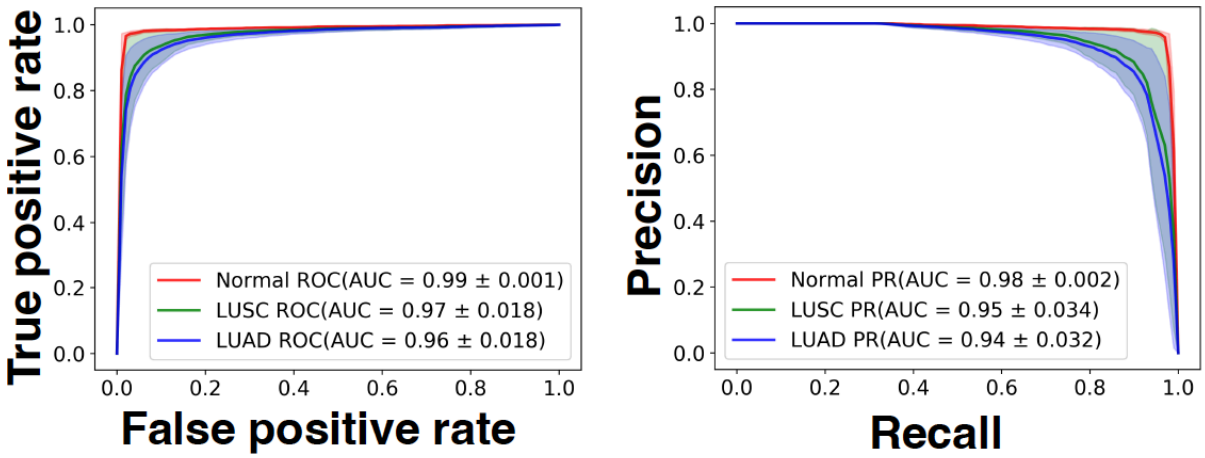

Figure 3: Classification Performance. Receiver Operating Characteristic (ROC) and Precision-Recall (PR) curves showcasing the performance of GRAPE-Net towards multi-class classification on CPTAC external testing dataset. The area under the curve (AUC) score for each label (Normal, LUAD, LUSC) is provided for the ROC and PR curves respectively.

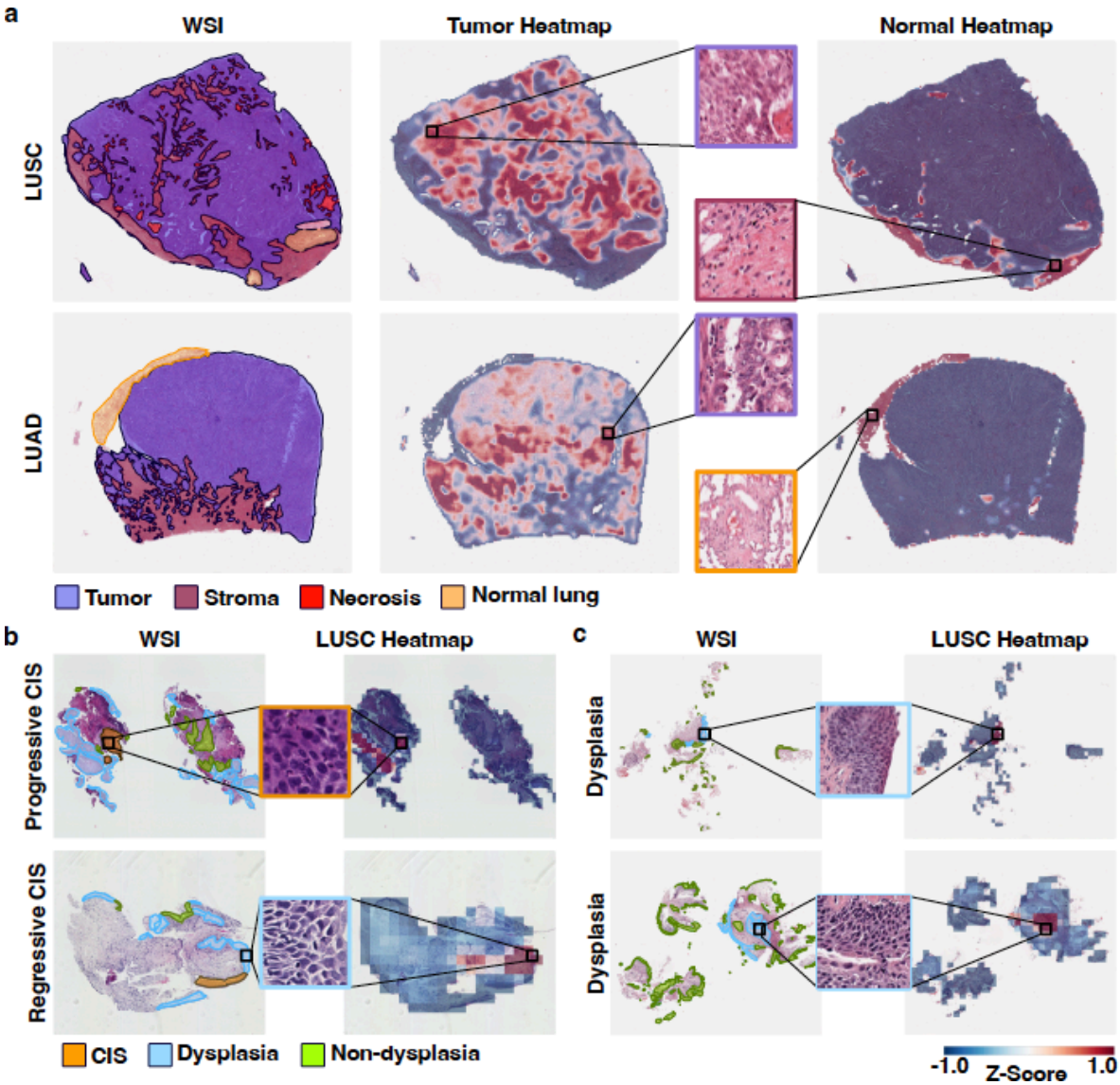

Figure 4: GRAPE-Net identifies tissue regions that correspond with pathologic annotations. (a) The network identified regions annotated as tumor and normal on LUAD and LUSC WSIs from CPTAC. **(b, c)** The network was also used to classify PMLs as one of the three labels. The LUSC-specific heatmaps for PMLs predicted to be LUSC identified regions of dysplasia and CIS as well as other regions that are likely contributing to its ability to separate CIS progressors from CIS regressors.

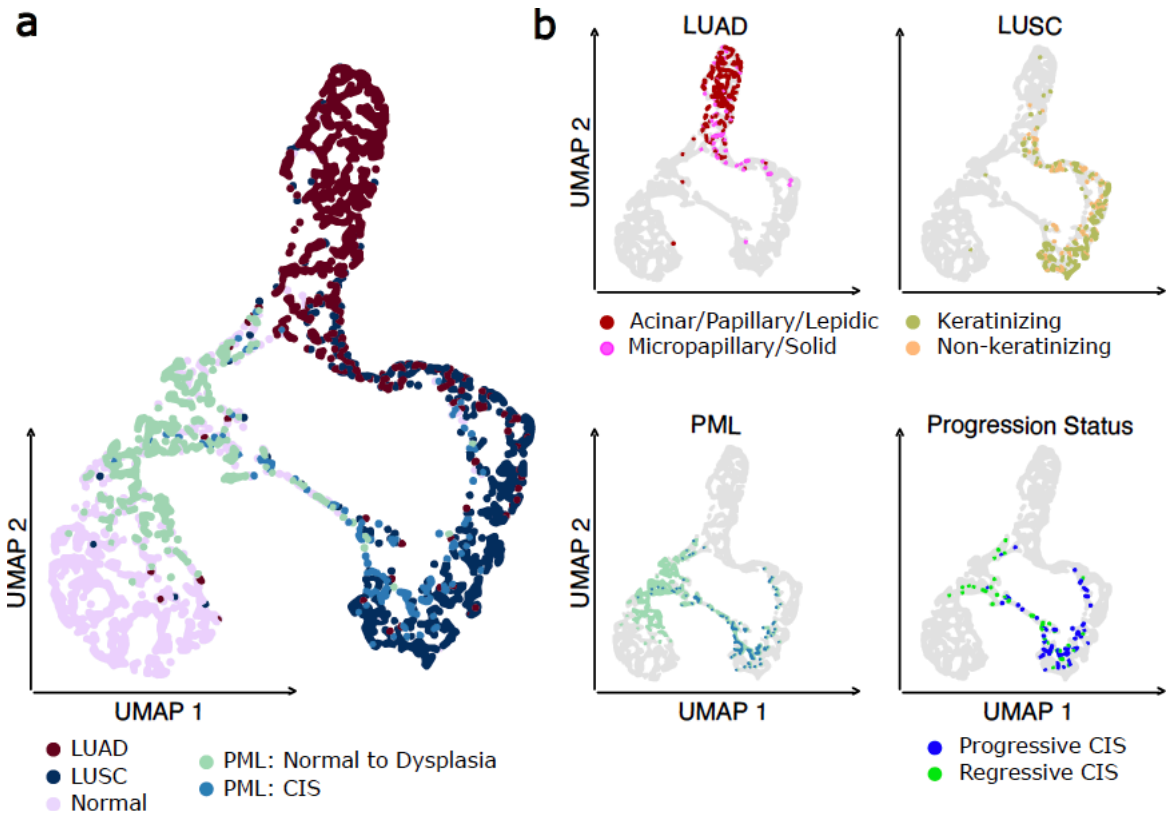

Figure 5: Stratification of lung tumors and PMLs relates to histologic features and outcome. UMAP plots of CPTAC, UCL, and Roswell WSI features stratified samples from normal to invasive carcinoma. The model separated LUAD and LUSC WSIs by tumor histologic patterns and CIS PMLs by outcome.

References

1. Beane JE, Mazzilli SA, Campbell JD, Duclos G, Krysan K, Moy C, Perdomo C, Schaffer M, Liu G, Zhang S, Liu H, Vick J, Dhillon SS, Platero SJ, Dubinett SM, Stevenson C, Reid ME, Lenburg ME, Spira AE: Molecular subtyping reveals immune alterations associated with progression of bronchial premalignant lesions. Nat Commun, Springer Science and Business Media LLC, 2019, 10:1856.

2. Merrick DT, Edwards MG, Franklin WA, Sugita M, Keith RL, Miller YE, Friedman MB, Dwyer-Nield LD, Tennis MA, O'Keefe MC, Donald EJ, Malloy JM, van Bokhoven A, Wilson S, Koch PJ, O'Shea C, Coldren C, Orlicky DJ, Lu X, Baron AE, Hickey G, Kennedy TC, Powell R, Heasley L, Bunn PA, Geraci M, Nemenoff RA: Altered cell-cycle control, inflammation, and adhesion in high-risk persistent bronchial dysplasia. Cancer Res, American Association for Cancer Research (AACR), 2018, 78:4971–4983.

3. Mascaux C, Angelova M, Vasaturo A, Beane J, Hijazi K, Anthoine G, Buttard B, Rothe F, Willard-Gallo K, Haller A, Ninane V, Burny A, Sculier J-P, Spira A, Galon J: Immune evasion before tumour invasion in early lung squamous carcinogenesis. Nature, Springer Science and Business Media LLC, 2019, 571:570–575.

4. Pennycuick A, Teixeira VH, AbdulJabbar K, Raza SEA, Lund T, Akarca AU, Rosenthal R, Kalinke L, Chandrasekharan DP, Pipinikas CP, Lee-Six H, Hynds RE, Gowers KHC, Henry JY, Millar FR, Hagos YB, Denais C, Falzon M, Moore DA, Antoniou S, Durrenberger PF, Furness AJ, Carroll B, Marceaux C, Asselin-Labat M-L, Larson W, Betts C, Coussens LM, Thakrar RM, George J, Swanton C, Thirlwell C, Campbell PJ, Marafioti T, Yuan Y, Quezada SA, McGranahan N, Janes SM: Immune surveillance in clinical regression of preinvasive squamous cell lung cancer. Cancer Discov, American Association for Cancer Research (AACR), 2020, 10:1489–1499.

5. Ning B, Tilston-Lunel AM, Simonetti J, Hicks-Berthet J, Matschulat A, Pfefferkorn R, Spira A, Edwards M, Mazzilli S, Lenburg ME, Beane JE, Varelas X: Convergence of YAP/TAZ, TEAD and TP63 activity is associated with bronchial premalignant severity and progression. J Exp Clin Cancer Res, Springer Science and Business Media LLC, 2023, 42:116.

6. Rozenblatt-Rosen O, Regev A, Oberdoerffer P, Nawy T, Hupalowska A, Rood JE, Ashenberg O, Cerami E, Coffey RJ, Demir E, Ding L, Esplin ED, Ford JM, Goecks J, Ghosh S, Gray JW, Guinney J, Hanlon SE, Hughes SK, Hwang ES, Iacobuzio-Donahue CA, Jané-Valbuena J, Johnson BE, Lau KS, Lively T, Mazzilli SA, Pe'er D, Santagata S, Shalek AK, Schapiro D, Snyder MP, Sorger PK, Spira AE, Srivastava S, Tan K, West RB, Williams EH, Human Tumor Atlas Network: The Human Tumor Atlas Network: Charting Tumor Transitions across Space and Time at Single-Cell Resolution. Cell 2020, 181:236–249.

7. TCGA Research Network, "The cancer genome atlas program". Available from: https://www.cancer.gov/tcga.

8. Edwards NJ, Oberti M, Thangudu RR, Cai S, McGarvey PB, Jacob S, Madhavan S, Ketchum KA: The CPTAC Data Portal: A Resource for Cancer Proteomics Research. J Proteome Res 2015, 14:2707–2713.

9. Otsu N: A threshold selection method from gray-level histograms. IEEE Trans Syst Man Cybern, Institute of Electrical and Electronics Engineers (IEEE), 1979, 9:62–66.

10. Wang X, Yang S, Zhang J, Wang M, Zhang J, Yang W, Huang J, Han X: Transformer-based unsupervised contrastive learning for histopathological image classification. Med Image Anal 2022, 81:102559.

11. Liu Z, Lin Y, Cao Y, Hu H, Wei Y, Zhang Z, Lin S, Guo B: Swin Transformer: Hierarchical Vision Transformer using Shifted Windows [Internet]. arXiv [cs.CV]. 2021, . Available from: http://arxiv.org/abs/2103.14030

12. Xu K, Hu W, Leskovec J, Jegelka S: How Powerful are Graph Neural Networks? [Internet]. arXiv [cs.LG]. 2018, . Available from: http://arxiv.org/abs/1810.00826

13. Jaegle A, Gimeno F, Brock A, Zisserman A, Vinyals O, Carreira J: Perceiver: General Perception with Iterative Attention [Internet]. arXiv [cs.CV]. 2021, . Available from: http://arxiv.org/abs/2103.03206

14. Vaswani A, Shazeer N, Parmar N, Uszkoreit J, Jones L, Gomez AN, Kaiser L, Polosukhin I: Attention is all you need [Internet]. arXiv [cs.CL]. 2017 [cited 2024 Feb 23], . Available from: http://arxiv.org/abs/1706.03762

15. Zheng Y, Gindra RH, Green EJ, Burks EJ, Betke M, Beane JE, Kolachalama VB: A Graph-Transformer for Whole Slide Image Classification. IEEE Trans Med Imaging 2022, 41:3003–3015.

16. Buterez D, Janet JP, Kiddle SJ, Oglic D, Liò P: Graph Neural Networks with Adaptive Readouts [Internet]. arXiv [cs.LG]. 2022, . Available from: http://arxiv.org/abs/2211.04952

17. Bianchi FM, Grattarola D, Alippi C: Spectral clustering with Graph Neural Networks for graph pooling [Internet]. arXiv [cs.LG]. 2019 [cited 2024 Feb 23], . Available from: http://arxiv.org/abs/1907.00481

18. Dosovitskiy A, Beyer L, Kolesnikov A, Weissenborn D, Zhai X, Unterthiner T, Dehghani M, Minderer M, Heigold G, Gelly S, Uszkoreit J, Houlsby N: An Image is Worth 16x16 Words: Transformers for Image Recognition at Scale [Internet]. arXiv [cs.CV]. 2020, . Available from: http://arxiv.org/abs/2010.11929

19. Kingma DP, Ba J: Adam: A Method for Stochastic Optimization [Internet]. arXiv [cs.LG]. 2014, . Available from: http://arxiv.org/abs/1412.6980

20. McInnes L, Healy J, Melville J: UMAP: Uniform Manifold Approximation and Projection for Dimension Reduction [Internet]. arXiv [stat.ML]. 2018, . Available from: http://arxiv.org/abs/1802.03426

21. Chefer H, Gur S, Wolf L: Generic Attention-model Explainability for Interpreting Bi-Modal and Encoder-Decoder Transformers [Internet]. arXiv [cs.CV]. 2021, . Available from: http://arxiv.org/abs/2103.15679

22. Wolf FA, Angerer P, Theis FJ: SCANPY: large-scale single-cell gene expression data analysis. Genome Biol 2018, 19:15.

23. Kadota K, Nitadori J-I, Rekhtman N, Jones DR, Adusumilli PS, Travis WD: Reevaluation and reclassification of resected lung carcinomas originally diagnosed as squamous cell carcinoma using immunohistochemical analysis. Am J Surg Pathol 2015, 39:1170–1180.

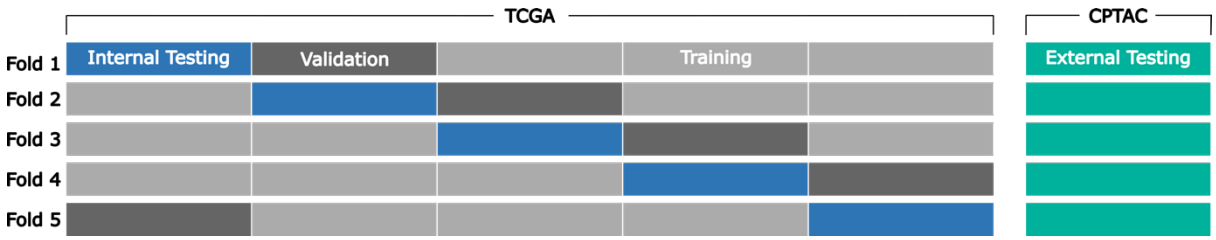

Supplementary Figure 1: Cross validation protocol. In addition to following the 5 fold cross-validation protocol for training, we also cycle through an unseen internal testing set every fold, to get an unbiased perspective of the model performance. Following the cross-validation, the model is also then tested on an external test set.

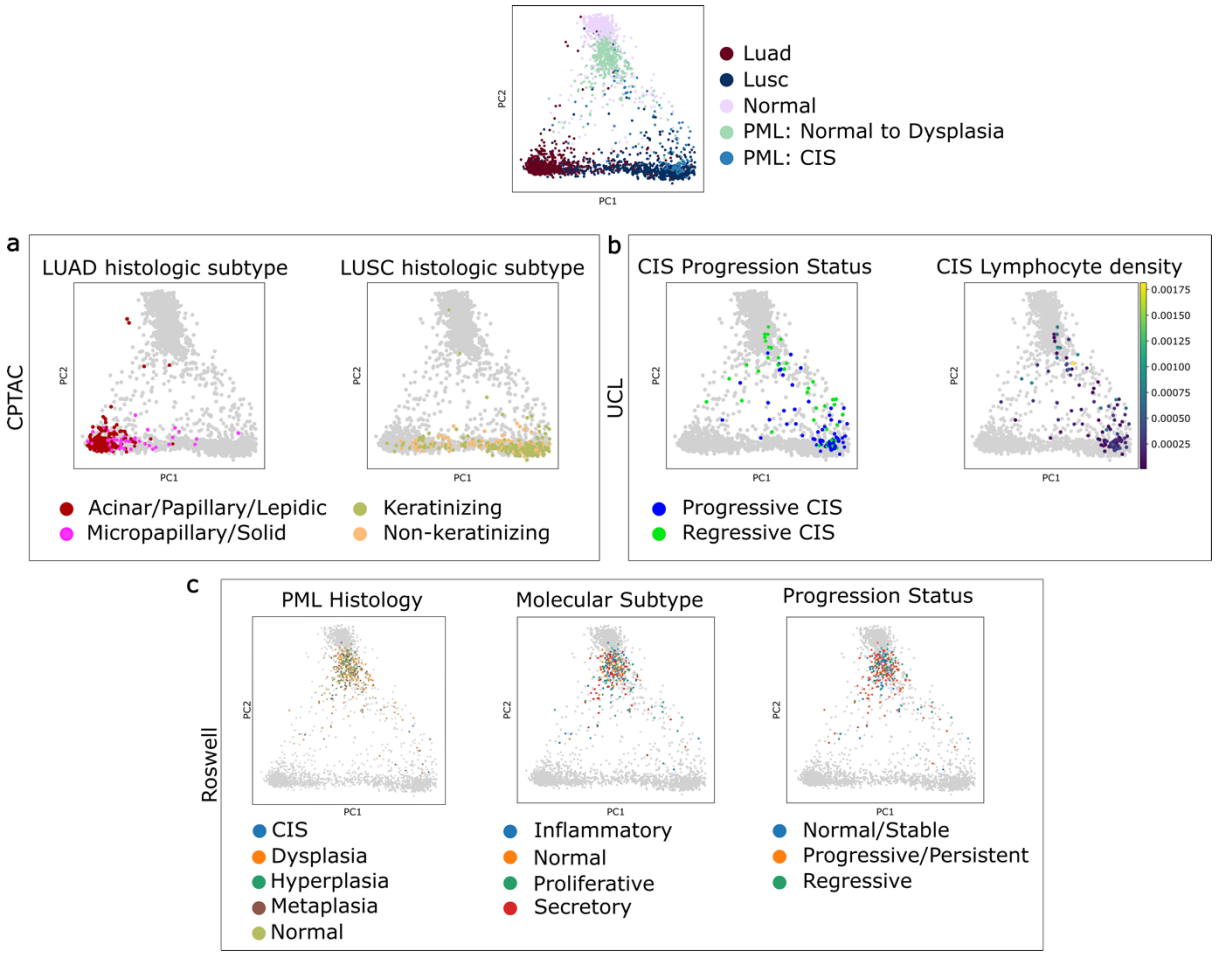

Supplementary Figure 2: Principal component analysis of lung tumor and premalignant lesions samples. Scatterplots of the first 2 principal components calculated using the final model-derived features across the same samples used for UMAP analysis in Figure 1. (a) Principal component analysis (PCA) plots with CPTAC samples highlighted by tumor subtype (b) PCA plots with UCL samples highlighted by progression status and lymphocyte count (c) PCA plots with Roswell samples highlighted by histologic grade, molecular subtype, and progression status.

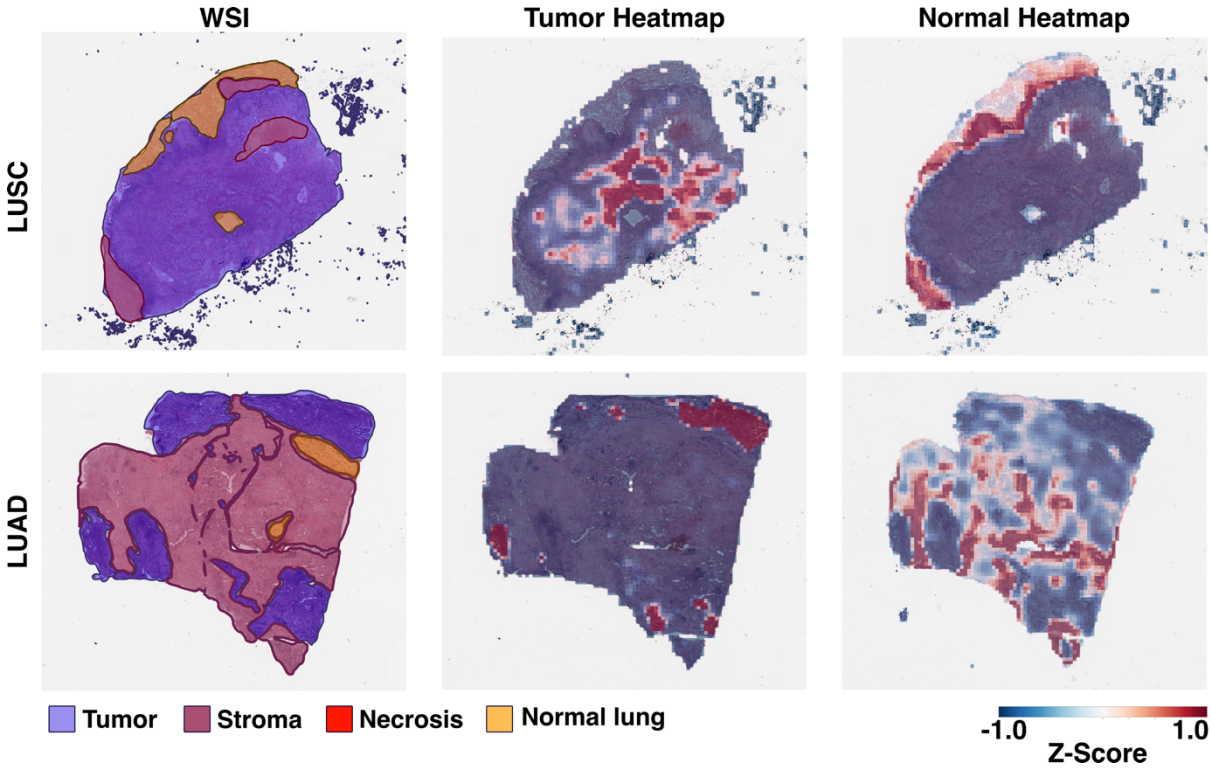

Supplementary Figure 3: Representative heatmaps of a LUAD and a LUSC case from CPTAC. The proce- dure for explanation visualizations is identical to Figure 2a. WSIs, their overlayed pathologist annotations (1st column) and respective tumor-specific (2nd column) and normal-specific heatmaps (3rd column) are shown for tumor resection samples from CPTAC cohort (LUSC, upper row and LUAD, bottom row). We observe a strong overlap between the tumor annotations and the tumor-specific heatmaps. Likewise, there is a strong overlap between stromal, necrotic and normal lung annotations and normal-specific heatmaps from GRAPE-Net, showing the network is able to understand the tissue region morphology well.

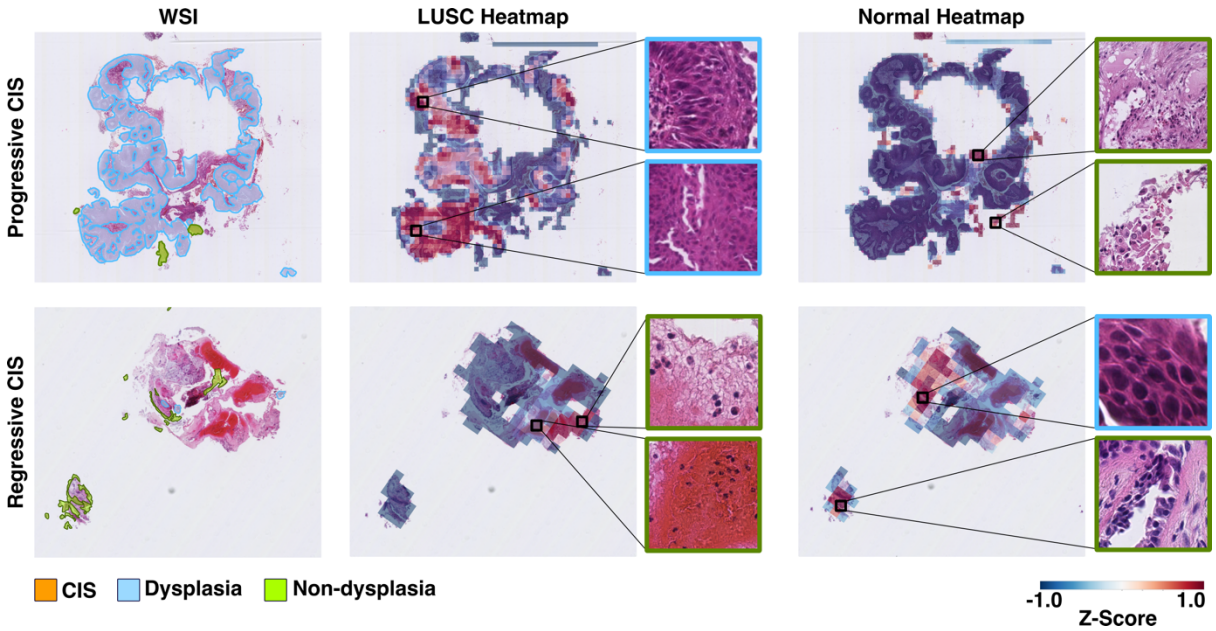

Supplementary Figure 4: Additional examples of heatmaps generated for UCL samples. The procedure for explanation visualizations is identical to Figure 2b. WSIs, their overlayed pathologist annotations (1st column) and respective LUSC-specific (2nd column) and normal-specific heatmaps (3rd column) are shown for endobronchial premalignant biopsies from UCL. We observe a strong overlap between the dysplasia annotations and LUSC-specific heatmaps in progressive cases but not in regressive cases.

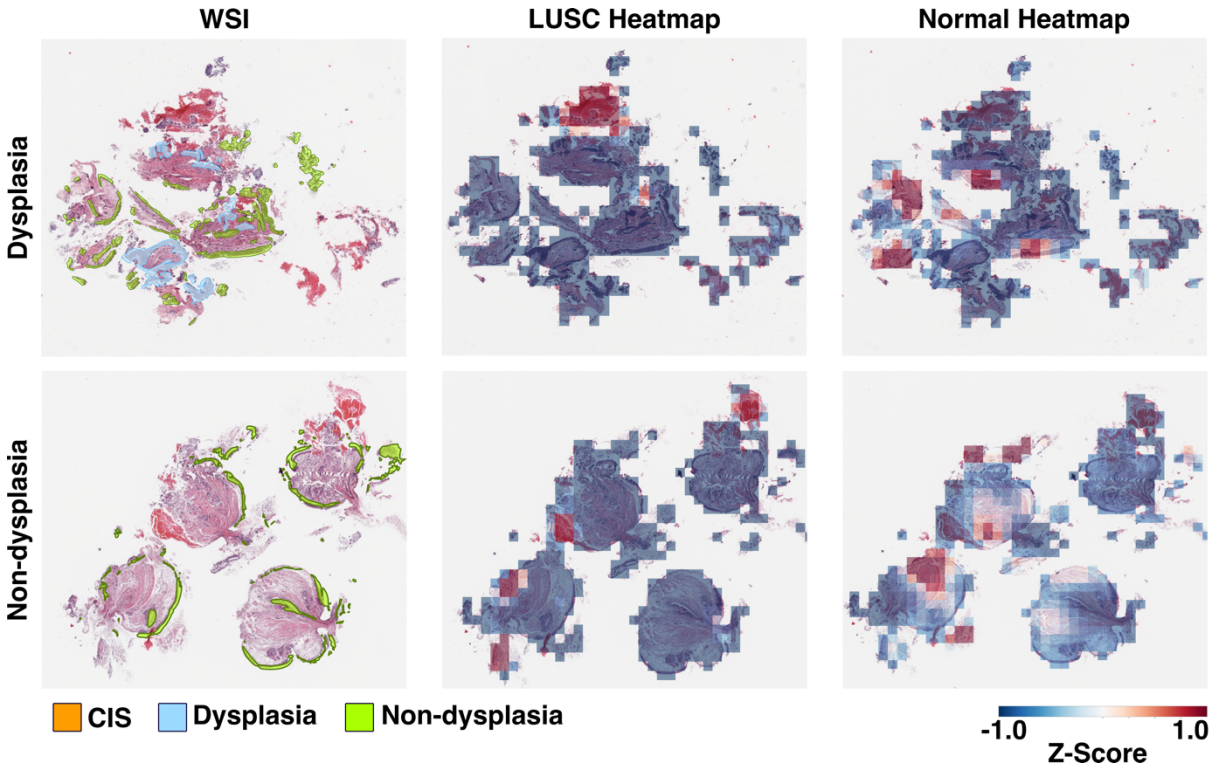

Supplementary Figure 5: Additional examples of heatmaps generated for Roswell samples: The procedure for explanation visualizations is identical to Fig 2c. WSIs, their overlayed pathologist annotations (1st column) and respective LUSC-specific (2nd column) and normal-specific heatmaps (3rd column) are shown for endobronchial premalignant biopsies from Roswell (top row, a case of with dysplasia regions and bottom row, a case without any regions of dsyplasia) predicted by the GPN to be normal. In cases predicted by the GPN to be normal, the GPN has diculty identifying the small regions of dysplasia with subtle abberrant epithelial changes.

PCGA Sample IDs

FileName	HTANBiospecimenID	HTANFileID
PCGA-01-0001-029-20126-01119BX.svs	HTA3_0001_1301119	HTA3_0001_1901119
PCGA-01-0001-037-19118-00482BX.svs	HTA3_0001_1300482	HTA3_0001_1900482
PCGA-01-0001-037-19300-00589BX.svs	HTA3_0001_1300589	HTA3_0001_1900589
PCGA-01-0001-037-19762-00898BX.svs	HTA3_0001_1300898	HTA3_0001_1900898
PCGA-01-0001-037-20126-01120BX.svs	HTA3_0001_1301120	HTA3_0001_1901120
PCGA-01-0001-050-15539-90001BX.svs	HTA3_0001_1390001	HTA3_0001_1990001
PCGA-01-0001-050-16918-90004BX.svs	HTA3_0001_1390004	HTA3_0001_1990004
PCGA-01-0001-050-19118-90002BX.svs	HTA3_0001_1390002	HTA3_0001_1990002
PCGA-01-0001-050-19300-90003BX.svs	HTA3_0001_1390003	HTA3_0001_1990003
PCGA-01-0001-050-19762-00903BX.svs	HTA3_0001_1300903	HTA3_0001_1900903
PCGA-01-0001-070-19118-90005BX.svs	HTA3_0001_1390005	HTA3_0001_1990005
PCGA-01-0001-070-19300-00587BX.svs	HTA3_0001_1300587	HTA3_0001_1900587
PCGA-01-0001-070-20126-01117BX.svs	HTA3_0001_1301117	HTA3_0001_1901117
PCGA-01-0001-074-19300-00586BX.svs	HTA3_0001_1300586	HTA3_0001_1900586

PCGA-01-0001-074-20126-01116BX.svs	HTA3_0001_1301116	HTA3_0001_1901116
PCGA-01-0001-074-20343-01315BX.svs	HTA3_0001_1301315	HTA3_0001_1901315
PCGA-01-0001-076-19300-00585BX.svs	HTA3_0001_1300585	HTA3_0001_1900585
PCGA-01-0001-076-20343-01314BX.svs	HTA3_0001_1301314	HTA3_0001_1901314
PCGA-01-0001-077-20126-01115BX.svs	HTA3_0001_1301115	HTA3_0001_1901115
PCGA-01-0001-082-19118-00480BX.svs	HTA3_0001_1300480	HTA3_0001_1900480
PCGA-01-0001-089-19118-00481BX.svs	HTA3_0001_1300481	HTA3_0001_1900481
PCGA-01-0001-089-19300-00588BX.svs	HTA3_0001_1300588	HTA3_0001_1900588
PCGA-01-0001-089-19762-00900BX.svs	HTA3_0001_1300900	HTA3_0001_1900900
PCGA-01-0001-089-20126-01118BX.svs	HTA3_0001_1301118	HTA3_0001_1901118
PCGA-01-0002-021-24062-00441BX.svs	HTA3_0002_1300441	HTA3_0002_1900441
PCGA-01-0002-077-24062-00442BX.svs	HTA3_0002_1300442	HTA3_0002_1900442
PCGA-01-0003-061-23883-90065BX.svs	HTA3_0003_1390065	HTA3_0003_1990065
PCGA-01-0003-061-24282-00694BX.svs	HTA3_0003_1300694	HTA3_0003_1900694
PCGA-01-0003-089-23883-90064BX.svs	HTA3_0003_1390064	HTA3_0003_1990064

PCGA-01-0003-089-24282-00693BX.svs	HTA3_0003_1300693	HTA3_0003_1900693
PCGA-01-0003-089-24730-00947BX.svs	HTA3_0003_1300947	HTA3_0003_1900947
PCGA-01-0004-050-25544-90067BX.svs	HTA3_0004_1390067	HTA3_0004_1990067
PCGA-01-0004-050-25733-90068BX.svs	HTA3_0004_1390068	HTA3_0004_1990068
PCGA-01-0004-050-26477-90006BX.svs	HTA3_0004_1390006	HTA3_0004_1990006
PCGA-01-0004-050-26687-90007BX.svs	HTA3_0004_1390007	HTA3_0004_1990007
PCGA-01-0004-050-27317-00606BX.svs	HTA3_0004_1300606	HTA3_0004_1900606
PCGA-01-0004-089-27317-00604BX.svs	HTA3_0004_1300604	HTA3_0004_1900604
PCGA-01-0004-093-26477-90008BX.svs	HTA3_0004_1390008	HTA3_0004_1990008
PCGA-01-0004-093-26687-90009BX.svs	HTA3_0004_1390009	HTA3_0004_1990009
PCGA-01-0004-093-27317-00605BX.svs	HTA3_0004_1300605	HTA3_0004_1900605
PCGA-01-0005-019-16929-00325BX.svs	HTA3_0005_1300325	HTA3_0005_1900325
PCGA-01-0005-019-17489-00727BX.svs	HTA3_0005_1300727	HTA3_0005_1900727
PCGA-01-0006-037-20238-00776BX.svs	HTA3_0006_1300776	HTA3_0006_1900776
PCGA-01-0006-037-21015-01279BX.svs	HTA3_0006_1301279	HTA3_0006_1901279

PCGA-01-0006-084-19783-00447BX.svs	HTA3_0006_1300447	HTA3_0006_1900447
PCGA-01-0007-048-18033-00455BX.svs	HTA3_0007_1300455	HTA3_0007_1900455
PCGA-01-0007-050-18033-00456BX.svs	HTA3_0007_1300456	HTA3_0007_1900456
PCGA-01-0007-050-18131-00528BX.svs	HTA3_0007_1300528	HTA3_0007_1900528
PCGA-01-0007-089-18033-00453BX.svs	HTA3_0007_1300453	HTA3_0007_1900453
PCGA-01-0007-089-18131-00526BX.svs	HTA3_0007_1300526	HTA3_0007_1900526
PCGA-01-0007-093-18131-00527BX.svs	HTA3_0007_1300527	HTA3_0007_1900527
PCGA-01-0008-045-21682-00840BX.svs	HTA3_0008_1300840	HTA3_0008_1900840
PCGA-01-0008-050-21682-00841BX.svs	HTA3_0008_1300841	HTA3_0008_1900841
PCGA-01-0008-050-22263-01196BX.svs	HTA3_0008_1301196	HTA3_0008_1901196
PCGA-01-0008-074-21682-00837BX.svs	HTA3_0008_1300837	HTA3_0008_1900837
PCGA-01-0008-074-22263-01191BX.svs	HTA3_0008_1301191	HTA3_0008_1901191
PCGA-01-0008-089-21115-00418BX.svs	HTA3_0008_1300418	HTA3_0008_1900418
PCGA-01-0008-089-21682-00838BX.svs	HTA3_0008_1300838	HTA3_0008_1900838
PCGA-01-0008-089-22263-01194BX.svs	HTA3_0008_1301194	HTA3_0008_1901194

PCGA-01-0009-053-23126-00557BX.svs	HTA3_0009_1300557	HTA3_0009_1900557
PCGA-01-0009-053-23497-00844BX.svs	HTA3_0009_1300844	HTA3_0009_1900844
PCGA-01-0009-053-23882-00991BX.svs	HTA3_0009_1300991	HTA3_0009_1900991
PCGA-01-0009-053-24085-01207BX.svs	HTA3_0009_1301207	HTA3_0009_1901207
PCGA-01-0009-061-23126-00558BX.svs	HTA3_0009_1300558	HTA3_0009_1900558
PCGA-01-0009-061-23497-00845BX.svs	HTA3_0009_1300845	HTA3_0009_1900845
PCGA-01-0009-061-23882-00992BX.svs	HTA3_0009_1300992	HTA3_0009_1900992
PCGA-01-0009-092-23497-00846BX.svs	HTA3_0009_1300846	HTA3_0009_1900846
PCGA-01-0009-092-24085-01209BX.svs	HTA3_0009_1301209	HTA3_0009_1901209
PCGA-01-0009-093-21241-90010BX.svs	HTA3_0009_1390010	HTA3_0009_1990010
PCGA-01-0010-048-19599-90011BX.svs	HTA3_0010_1390011	HTA3_0010_1990011
PCGA-01-0010-048-19900-90012BX.svs	HTA3_0010_1390012	HTA3_0010_1990012
PCGA-01-0010-050-19599-00505BX.svs	HTA3_0010_1300505	HTA3_0010_1900505
PCGA-01-0010-050-19599-90013BX.svs	HTA3_0010_1390013	HTA3_0010_1990013
PCGA-01-0010-050-19900-90014BX.svs	HTA3_0010_1390014	HTA3_0010_1990014

PCGA-01-0010-089-19599-00503BX.svs	HTA3_0010_1300503	HTA3_0010_1900503
PCGA-01-0010-089-19599-90061BX.svs	HTA3_0010_1390061	HTA3_0010_1990061
PCGA-01-0010-089-19900-00700BX.svs	HTA3_0010_1300700	HTA3_0010_1900700
PCGA-01-0010-089-19900-90062BX.svs	HTA3_0010_1390062	HTA3_0010_1990062
PCGA-01-0010-094-19599-00504BX.svs	HTA3_0010_1300504	HTA3_0010_1900504
PCGA-01-0010-094-19900-00701BX.svs	HTA3_0010_1300701	HTA3_0010_1900701
PCGA-01-0011-050-26439-00341BX.svs	HTA3_0011_1300341	HTA3_0011_1900341
PCGA-01-0011-050-26558-00433BX.svs	HTA3_0011_1300433	HTA3_0011_1900433
PCGA-01-0011-050-26740-00567BX.svs	HTA3_0011_1300567	HTA3_0011_1900567
PCGA-01-0011-089-26439-00340BX.svs	HTA3_0011_1300340	HTA3_0011_1900340
PCGA-01-0011-089-26558-00432BX.svs	HTA3_0011_1300432	HTA3_0011_1900432
PCGA-01-0011-089-26740-90015BX.svs	HTA3_0011_1390015	HTA3_0011_1990015
PCGA-01-0012-050-21101-00736BX.svs	HTA3_0012_1300736	HTA3_0012_1900736
PCGA-01-0012-050-21836-01253BX.svs	HTA3_0012_1301253	HTA3_0012_1901253
PCGA-01-0014-010-19671-90020BX.svs	HTA3_0014_1390020	HTA3_0014_1990020

PCGA-01-0014-010-20660-00748BX.svs	HTA3_0014_1300748	HTA3_0014_1900748
PCGA-01-0014-011-19323-90017BX.svs	HTA3_0014_1390017	HTA3_0014_1990017
PCGA-01-0014-011-20177-00394BX.svs	HTA3_0014_1300394	HTA3_0014_1900394
PCGA-01-0014-011-20660-00747BX.svs	HTA3_0014_1300747	HTA3_0014_1900747
PCGA-01-0014-011-20660-90018BX.svs	HTA3_0014_1390018	HTA3_0014_1990018
PCGA-01-0014-053-20177-00393BX.svs	HTA3_0014_1300393	HTA3_0014_1900393
PCGA-01-0014-053-20177-90023BX.svs	HTA3_0014_1390023	HTA3_0014_1990023
PCGA-01-0014-053-20660-00745BX.svs	HTA3_0014_1300745	HTA3_0014_1900745
PCGA-01-0014-089-20660-00744BX.svs	HTA3_0014_1300744	HTA3_0014_1900744
PCGA-01-0014-093-20177-90021BX.svs	HTA3_0014_1390021	HTA3_0014_1990021
PCGA-01-0015-011-16303-00402BX.svs	HTA3_0015_1300402	HTA3_0015_1900402
PCGA-01-0015-011-16541-00571BX.svs	HTA3_0015_1300571	HTA3_0015_1900571
PCGA-01-0015-011-17129-00932BX.svs	HTA3_0015_1300932	HTA3_0015_1900932
PCGA-01-0015-011-17638-01327BX.svs	HTA3_0015_1301327	HTA3_0015_1901327
PCGA-01-0015-025-16541-00570BX.svs	HTA3_0015_1300570	HTA3_0015_1900570

PCGA-01-0015-025-16954-00864BX.svs	HTA3_0015_1300864	HTA3_0015_1900864
PCGA-01-0016-025-22821-90024BX.svs	HTA3_0016_1390024	HTA3_0016_1990024
PCGA-01-0016-025-23045-90025BX.svs	HTA3_0016_1390025	HTA3_0016_1990025
PCGA-01-0016-050-22821-00509BX.svs	HTA3_0016_1300509	HTA3_0016_1900509
PCGA-01-0016-050-23045-00647BX.svs	HTA3_0016_1300647	HTA3_0016_1900647
PCGA-01-0017-052-19883-00473BX.svs	HTA3_0017_1300473	HTA3_0017_1900473
PCGA-01-0017-052-19883-90030BX.svs	HTA3_0017_1390030	HTA3_0017_1990030
PCGA-01-0017-052-20261-00732BX.svs	HTA3_0017_1300732	HTA3_0017_1900732
PCGA-01-0017-052-20261-90028BX.svs	HTA3_0017_1390028	HTA3_0017_1990028
PCGA-01-0017-052-20422-00850BX.svs	HTA3_0017_1300850	HTA3_0017_1900850
PCGA-01-0017-052-20422-90029BX.svs	HTA3_0017_1390029	HTA3_0017_1990029
PCGA-01-0017-089-19883-00472BX.svs	HTA3_0017_1300472	HTA3_0017_1900472
PCGA-01-0017-089-20261-00731BX.svs	HTA3_0017_1300731	HTA3_0017_1900731
PCGA-01-0017-089-20422-00849BX.svs	HTA3_0017_1300849	HTA3_0017_1900849
PCGA-01-0018-050-21752-00496BX.svs	HTA3_0018_1300496	HTA3_0018_1900496

PCGA-01-0018-050-21990-00651BX.svs	HTA3_0018_1300651	HTA3_0018_1900651
PCGA-01-0018-050-22732-01146BX.svs	HTA3_0018_1301146	HTA3_0018_1901146
PCGA-01-0018-074-21752-00494BX.svs	HTA3_0018_1300494	HTA3_0018_1900494
PCGA-01-0018-074-21990-00650BX.svs	HTA3_0018_1300650	HTA3_0018_1900650
PCGA-01-0018-074-22732-01145BX.svs	HTA3_0018_1301145	HTA3_0018_1901145
PCGA-01-0020-048-23497-00370BX.svs	HTA3_0020_1300370	HTA3_0020_1900370
PCGA-01-0020-048-23497-90031BX.svs	HTA3_0020_1390031	HTA3_0020_1990031
PCGA-01-0020-048-24050-00784BX.svs	HTA3_0020_1300784	HTA3_0020_1900784
PCGA-01-0020-048-24050-90032BX.svs	HTA3_0020_1390032	HTA3_0020_1990032
PCGA-01-0020-094-23497-00367BX.svs	HTA3_0020_1300367	HTA3_0020_1900367
PCGA-01-0020-094-23497-90033BX.svs	HTA3_0020_1390033	HTA3_0020_1990033
PCGA-01-0020-094-24050-00783BX.svs	HTA3_0020_1300783	HTA3_0020_1900783
PCGA-01-0020-094-24050-90034BX.svs	HTA3_0020_1390034	HTA3_0020_1990034
PCGA-01-0021-010-19826-00723BX.svs	HTA3_0021_1300723	HTA3_0021_1900723
PCGA-01-0021-010-20218-00943BX.svs	HTA3_0021_1300943	HTA3_0021_1900943

PCGA-01-0021-025-19266-00319BX.svs	HTA3_0021_1300319	HTA3_0021_1900319
PCGA-01-0021-025-20218-00942BX.svs	HTA3_0021_1300942	HTA3_0021_1900942
PCGA-01-0021-025-20449-01091BX.svs	HTA3_0021_1301091	HTA3_0021_1901091
PCGA-01-0021-025-20687-01310BX.svs	HTA3_0021_1301310	HTA3_0021_1901310
PCGA-01-0021-050-19434-00465BX.svs	HTA3_0021_1300465	HTA3_0021_1900465
PCGA-01-0021-050-19826-00724BX.svs	HTA3_0021_1300724	HTA3_0021_1900724
PCGA-01-0021-050-20218-00944BX.svs	HTA3_0021_1300944	HTA3_0021_1900944
PCGA-01-0021-050-20449-01092BX.svs	HTA3_0021_1301092	HTA3_0021_1901092
PCGA-01-0021-050-20687-01311BX.svs	HTA3_0021_1301311	HTA3_0021_1901311
PCGA-01-0021-070-19266-90035BX.svs	HTA3_0021_1390035	HTA3_0021_1990035
PCGA-01-0021-070-19623-00581BX.svs	HTA3_0021_1300581	HTA3_0021_1900581
PCGA-01-0021-070-19623-90037BX.svs	HTA3_0021_1390037	HTA3_0021_1990037
PCGA-01-0021-070-19826-00720BX.svs	HTA3_0021_1300720	HTA3_0021_1900720
PCGA-01-0021-070-20218-00940BX.svs	HTA3_0021_1300940	HTA3_0021_1900940
PCGA-01-0021-070-20449-01089BX.svs	HTA3_0021_1301089	HTA3_0021_1901089

PCGA-01-0021-070-20687-01307BX.svs	HTA3_0021_1301307	HTA3_0021_1901307
PCGA-01-0021-088-19826-00721BX.svs	HTA3_0021_1300721	HTA3_0021_1900721
PCGA-01-0021-089-19266-90038BX.svs	HTA3_0021_1390038	HTA3_0021_1990038
PCGA-01-0021-089-19434-90039BX.svs	HTA3_0021_1390039	HTA3_0021_1990039
PCGA-01-0021-089-19623-00582BX.svs	HTA3_0021_1300582	HTA3_0021_1900582
PCGA-01-0021-089-19826-00722BX.svs	HTA3_0021_1300722	HTA3_0021_1900722
PCGA-01-0021-089-19826-90040BX.svs	HTA3_0021_1390040	HTA3_0021_1990040
PCGA-01-0021-089-20218-00941BX.svs	HTA3_0021_1300941	HTA3_0021_1900941
PCGA-01-0021-089-20687-01308BX.svs	HTA3_0021_1301308	HTA3_0021_1901308
PCGA-01-0022-070-20918-00468BX.svs	HTA3_0022_1300468	HTA3_0022_1900468
PCGA-01-0022-070-21548-00876BX.svs	HTA3_0022_1300876	HTA3_0022_1900876
PCGA-01-0022-070-21996-01169BX.svs	HTA3_0022_1301169	HTA3_0022_1901169
PCGA-01-0022-089-20918-00469BX.svs	HTA3_0022_1300469	HTA3_0022_1900469
PCGA-01-0022-089-21996-01170BX.svs	HTA3_0022_1301170	HTA3_0022_1901170
PCGA-01-0022-093-21548-00878BX.svs	HTA3_0022_1300878	HTA3_0022_1900878

PCGA-01-0022-093-21996-01171BX.svs	HTA3_0022_1301171	HTA3_0022_1901171
PCGA-01-0023-010-21429-00830BX.svs	HTA3_0023_1300830	HTA3_0023_1900830
PCGA-01-0023-025-20400-90041BX.svs	HTA3_0023_1390041	HTA3_0023_1990041
PCGA-01-0023-025-20764-90047BX.svs	HTA3_0023_1390047	HTA3_0023_1990047
PCGA-01-0023-026-21429-00827BX.svs	HTA3_0023_1300827	HTA3_0023_1900827
PCGA-01-0023-048-21429-00829BX.svs	HTA3_0023_1300829	HTA3_0023_1900829
PCGA-01-0023-050-20200-90043BX.svs	HTA3_0023_1390043	HTA3_0023_1990043
PCGA-01-0023-050-20246-90042BX.svs	HTA3_0023_1390042	HTA3_0023_1990042
PCGA-01-0023-050-20764-90044BX.svs	HTA3_0023_1390044	HTA3_0023_1990044
PCGA-01-0023-050-21429-00828BX.svs	HTA3_0023_1300828	HTA3_0023_1900828
PCGA-01-0023-061-21429-00826BX.svs	HTA3_0023_1300826	HTA3_0023_1900826
PCGA-01-0023-066-21429-00824BX.svs	HTA3_0023_1300824	HTA3_0023_1900824
PCGA-01-0023-070-20400-90048BX.svs	HTA3_0023_1390048	HTA3_0023_1990048
PCGA-01-0023-070-20764-90045BX.svs	HTA3_0023_1390045	HTA3_0023_1990045
PCGA-01-0023-089-21429-00825BX.svs	HTA3_0023_1300825	HTA3_0023_1900825

PCGA-01-0024-050-23686-00520BX.svs	HTA3_0024_1300520	HTA3_0024_1900520
PCGA-01-0024-050-24050-00780BX.svs	HTA3_0024_1300780	HTA3_0024_1900780
PCGA-01-0025-048-20884-00600BX.svs	HTA3_0025_1300600	HTA3_0025_1900600
PCGA-01-0025-048-21689-01106BX.svs	HTA3_0025_1301106	HTA3_0025_1901106
PCGA-01-0025-050-20576-00384BX.svs	HTA3_0025_1300384	HTA3_0025_1900384
PCGA-01-0025-050-20772-00541BX.svs	HTA3_0025_1300541	HTA3_0025_1900541
PCGA-01-0025-050-20884-00601BX.svs	HTA3_0025_1300601	HTA3_0025_1900601
PCGA-01-0025-050-21164-00807BX.svs	HTA3_0025_1300807	HTA3_0025_1900807
PCGA-01-0025-050-21689-01108BX.svs	HTA3_0025_1301108	HTA3_0025_1901108
PCGA-01-0025-070-20576-90049BX.svs	HTA3_0025_1390049	HTA3_0025_1990049
PCGA-01-0025-070-21164-90050BX.svs	HTA3_0025_1390050	HTA3_0025_1990050
PCGA-01-0025-074-20576-00383BX.svs	HTA3_0025_1300383	HTA3_0025_1900383
PCGA-01-0025-074-20772-00540BX.svs	HTA3_0025_1300540	HTA3_0025_1900540
PCGA-01-0025-074-20884-00599BX.svs	HTA3_0025_1300599	HTA3_0025_1900599
PCGA-01-0025-074-21164-00805BX.svs	HTA3_0025_1300805	HTA3_0025_1900805

PCGA-01-0025-074-21689-01105BX.svs	HTA3_0025_1301105	HTA3_0025_1901105
PCGA-01-0025-094-21164-00806BX.svs	HTA3_0025_1300806	HTA3_0025_1900806
PCGA-01-0025-094-21689-01107BX.svs	HTA3_0025_1301107	HTA3_0025_1901107
PCGA-01-0026-089-21752-00337BX.svs	HTA3_0026_1300337	HTA3_0026_1900337
PCGA-01-0026-089-22473-00859BX.svs	HTA3_0026_1300859	HTA3_0026_1900859
PCGA-01-0027-089-19515-00639BX.svs	HTA3_0027_1300639	HTA3_0027_1900639
PCGA-01-0028-041-23527-00757BX.svs	HTA3_0028_1300757	HTA3_0028_1900757
PCGA-01-0028-041-24262-01264BX.svs	HTA3_0028_1301264	HTA3_0028_1901264
PCGA-01-0028-050-23163-00491BX.svs	HTA3_0028_1300491	HTA3_0028_1900491
PCGA-01-0028-050-23527-00758BX.svs	HTA3_0028_1300758	HTA3_0028_1900758
PCGA-01-0028-050-24262-01265BX.svs	HTA3_0028_1301265	HTA3_0028_1901265
PCGA-01-0029-045-22412-00625BX.svs	HTA3_0029_1300625	HTA3_0029_1900625
PCGA-01-0029-045-22678-00814BX.svs	HTA3_0029_1300814	HTA3_0029_1900814
PCGA-01-0029-048-22090-00379BX.svs	HTA3_0029_1300379	HTA3_0029_1900379
PCGA-01-0029-048-22412-90051BX.svs	HTA3_0029_1390051	HTA3_0029_1990051

PCGA-01-0029-048-22678-00815BX.svs	HTA3_0029_1300815	HTA3_0029_1900815
PCGA-01-0029-050-22090-00380BX.svs	HTA3_0029_1300380	HTA3_0029_1900380
PCGA-01-0029-050-22678-00816BX.svs	HTA3_0029_1300816	HTA3_0029_1900816
PCGA-01-0029-061-22090-00378BX.svs	HTA3_0029_1300378	HTA3_0029_1900378
PCGA-01-0029-061-22412-00623BX.svs	HTA3_0029_1300623	HTA3_0029_1900623
PCGA-01-0029-061-22678-00812BX.svs	HTA3_0029_1300812	HTA3_0029_1900812
PCGA-01-0029-070-22090-00376BX.svs	HTA3_0029_1300376	HTA3_0029_1900376
PCGA-01-0029-070-22412-90052BX.svs	HTA3_0029_1390052	HTA3_0029_1990052
PCGA-01-0029-070-22678-00810BX.svs	HTA3_0029_1300810	HTA3_0029_1900810
PCGA-01-0029-089-22090-00377BX.svs	HTA3_0029_1300377	HTA3_0029_1900377
PCGA-01-0029-089-22412-00622BX.svs	HTA3_0029_1300622	HTA3_0029_1900622
PCGA-01-0029-093-22090-90054BX.svs	HTA3_0029_1390054	HTA3_0029_1990054
PCGA-01-0029-093-22412-00624BX.svs	HTA3_0029_1300624	HTA3_0029_1900624
PCGA-01-0029-093-22678-00813BX.svs	HTA3_0029_1300813	HTA3_0029_1900813
PCGA-01-0030-089-27868-00358BX.svs	HTA3_0030_1300358	HTA3_0030_1900358

PCGA-01-0031-021-24061-00664BX.svs	HTA3_0031_1300664	HTA3_0031_1900664
PCGA-01-0031-021-24726-01062BX.svs	HTA3_0031_1301062	HTA3_0031_1901062
PCGA-01-0031-050-23830-00537BX.svs	HTA3_0031_1300537	HTA3_0031_1900537
PCGA-01-0031-050-24061-00666BX.svs	HTA3_0031_1300666	HTA3_0031_1900666
PCGA-01-0031-050-24285-00856BX.svs	HTA3_0031_1300856	HTA3_0031_1900856
PCGA-01-0031-050-24726-01063BX.svs	HTA3_0031_1301063	HTA3_0031_1901063
PCGA-01-0031-053-24061-00665BX.svs	HTA3_0031_1300665	HTA3_0031_1900665
PCGA-01-0031-053-24285-00855BX.svs	HTA3_0031_1300855	HTA3_0031_1900855
PCGA-01-0031-053-24285-90057BX.svs	HTA3_0031_1390057	HTA3_0031_1990057
PCGA-01-0031-053-24726-01061BX.svs	HTA3_0031_1301061	HTA3_0031_1901061
PCGA-01-0031-066-23830-90055BX.svs	HTA3_0031_1390055	HTA3_0031_1990055
PCGA-01-0031-066-24061-90056BX.svs	HTA3_0031_1390056	HTA3_0031_1990056
PCGA-01-0031-074-24285-00854BX.svs	HTA3_0031_1300854	HTA3_0031_1900854
PCGA-01-0031-074-24726-01060BX.svs	HTA3_0031_1301060	HTA3_0031_1901060
PCGA-01-0032-088-24051-00544BX.svs	HTA3_0032_1300544	HTA3_0032_1900544

PCGA-01-0033-048-20582-00974BX.svs	HTA3_0033_1300974	HTA3_0033_1900974
PCGA-01-0033-048-20864-01248BX.svs	HTA3_0033_1301248	HTA3_0033_1901248
PCGA-01-0033-048-21079-01371BX.svs	HTA3_0033_1301371	HTA3_0033_1901371
PCGA-01-0033-050-20582-00977BX.svs	HTA3_0033_1300977	HTA3_0033_1900977
PCGA-01-0033-050-20864-01249BX.svs	HTA3_0033_1301249	HTA3_0033_1901249
PCGA-01-0033-061-20864-01246BX.svs	HTA3_0033_1301246	HTA3_0033_1901246
PCGA-01-0033-085-20864-01245BX.svs	HTA3_0033_1301245	HTA3_0033_1901245
PCGA-01-0033-085-21079-01370BX.svs	HTA3_0033_1301370	HTA3_0033_1901370
PCGA-01-0033-092-21079-01369BX.svs	HTA3_0033_1301369	HTA3_0033_1901369
PCGA-01-0034-050-22969-00918BX.svs	HTA3_0034_1300918	HTA3_0034_1900918
PCGA-01-0035-019-21168-01034BX.svs	HTA3_0035_1301034	HTA3_0035_1901034
PCGA-01-0035-019-21364-01259BX.svs	HTA3_0035_1301259	HTA3_0035_1901259
PCGA-01-0035-042-21168-01035BX.svs	HTA3_0035_1301035	HTA3_0035_1901035
PCGA-01-0035-042-21364-01260BX.svs	HTA3_0035_1301260	HTA3_0035_1901260
PCGA-01-0035-050-21168-01039BX.svs	HTA3_0035_1301039	HTA3_0035_1901039

PCGA-01-0035-061-21168-01037BX.svs	HTA3_0035_1301037	HTA3_0035_1901037
PCGA-01-0035-061-21364-01257BX.svs	HTA3_0035_1301257	HTA3_0035_1901257
PCGA-01-0035-074-21168-01036BX.svs	HTA3_0035_1301036	HTA3_0035_1901036
PCGA-01-0035-074-21364-01256BX.svs	HTA3_0035_1301256	HTA3_0035_1901256
PCGA-01-0035-093-21168-01038BX.svs	HTA3_0035_1301038	HTA3_0035_1901038
PCGA-01-0035-093-21364-01258BX.svs	HTA3_0035_1301258	HTA3_0035_1901258
PCGA-01-0036-048-21975-00298BX.svs	HTA3_0036_1300298	HTA3_0036_1900298
PCGA-01-0036-048-22885-00913BX.svs	HTA3_0036_1300913	HTA3_0036_1900913
PCGA-01-0036-050-22885-00914BX.svs	HTA3_0036_1300914	HTA3_0036_1900914
PCGA-01-0036-050-23647-01405BX.svs	HTA3_0036_1301405	HTA3_0036_1901405
PCGA-01-0036-089-21975-00297BX.svs	HTA3_0036_1300297	HTA3_0036_1900297
PCGA-01-0036-089-22885-00911BX.svs	HTA3_0036_1300911	HTA3_0036_1900911
PCGA-01-0036-089-23647-01404BX.svs	HTA3_0036_1301404	HTA3_0036_1901404
PCGA-01-0037-089-27849-00344BX.svs	HTA3_0037_1300344	HTA3_0037_1900344
PCGA-01-0037-089-28409-00751BX.svs	HTA3_0037_1300751	HTA3_0037_1900751

PCGA-01-0038-037-20756-00770BX.svs	HTA3_0038_1300770	HTA3_0038_1900770
PCGA-01-0038-037-21323-01075BX.svs	HTA3_0038_1301075	HTA3_0038_1901075
PCGA-01-0038-037-21699-01390BX.svs	HTA3_0038_1301390	HTA3_0038_1901390
PCGA-01-0038-048-21323-01076BX.svs	HTA3_0038_1301076	HTA3_0038_1901076
PCGA-01-0038-048-21699-01391BX.svs	HTA3_0038_1301391	HTA3_0038_1901391
PCGA-01-0038-050-20756-00771BX.svs	HTA3_0038_1300771	HTA3_0038_1900771
PCGA-01-0038-050-21323-01077BX.svs	HTA3_0038_1301077	HTA3_0038_1901077
PCGA-01-0038-050-21699-01392BX.svs	HTA3_0038_1301392	HTA3_0038_1901392
PCGA-01-0039-066-19554-01003BX.svs	HTA3_0039_1301003	HTA3_0039_1901003
PCGA-01-0039-076-19554-01002BX.svs	HTA3_0039_1301002	HTA3_0039_1901002
PCGA-01-0039-076-19757-01220BX.svs	HTA3_0039_1301220	HTA3_0039_1901220
PCGA-01-0039-089-19554-01004BX.svs	HTA3_0039_1301004	HTA3_0039_1901004
PCGA-01-0039-089-19757-01222BX.svs	HTA3_0039_1301222	HTA3_0039_1901222
PCGA-01-0039-093-19554-01005BX.svs	HTA3_0039_1301005	HTA3_0039_1901005
PCGA-01-0039-093-19757-01224BX.svs	HTA3_0039_1301224	HTA3_0039_1901224

PCGA-01-0040-050-19706-01100BX.svs	HTA3_0040_1301100	HTA3_0040_1901100
PCGA-01-0040-050-19895-01284BX.svs	HTA3_0040_1301284	HTA3_0040_1901284
PCGA-01-0040-093-19706-01098BX.svs	HTA3_0040_1301098	HTA3_0040_1901098
PCGA-01-0040-093-19895-01283BX.svs	HTA3_0040_1301283	HTA3_0040_1901283
PCGA-01-0041-050-21430-00796BX.svs	HTA3_0041_1300796	HTA3_0041_1900796
PCGA-01-0041-050-21703-00922BX.svs	HTA3_0041_1300922	HTA3_0041_1900922
PCGA-01-0041-050-22044-01183BX.svs	HTA3_0041_1301183	HTA3_0041_1901183
PCGA-01-0041-093-21430-00795BX.svs	HTA3_0041_1300795	HTA3_0041_1900795
PCGA-01-0041-093-21703-00919BX.svs	HTA3_0041_1300919	HTA3_0041_1900919
PCGA-01-0041-093-22044-01182BX.svs	HTA3_0041_1301182	HTA3_0041_1901182
PCGA-01-0042-010-23680-00906BX.svs	HTA3_0042_1300906	HTA3_0042_1900906
PCGA-01-0042-010-23911-01028BX.svs	HTA3_0042_1301028	HTA3_0042_1901028
PCGA-01-0042-048-23680-00907BX.svs	HTA3_0042_1300907	HTA3_0042_1900907
PCGA-01-0042-048-23911-01029BX.svs	HTA3_0042_1301029	HTA3_0042_1901029
PCGA-01-0043-037-21235-01043BX.svs	HTA3_0043_1301043	HTA3_0043_1901043

PCGA-01-0043-037-21599-01350BX.svs	HTA3_0043_1301350	HTA3_0043_1901350
PCGA-01-0043-085-21599-01349BX.svs	HTA3_0043_1301349	HTA3_0043_1901349
PCGA-01-0044-048-17646-44967BX.svs	HTA3_0044_1300967	HTA3_0044_1900967
PCGA-01-0044-048-17898-01132BX.svs	HTA3_0044_1301132	HTA3_0044_1901132
PCGA-01-0044-050-17646-44968BX.svs	HTA3_0044_1300968	HTA3_0044_1900968
PCGA-01-0044-050-17898-01133BX.svs	HTA3_0044_1301133	HTA3_0044_1901133
PCGA-01-0044-050-18295-01397BX.svs	HTA3_0044_1301397	HTA3_0044_1901397
PCGA-01-0044-070-16659-00293BX.svs	HTA3_0044_1300293	HTA3_0044_1900293
PCGA-01-0044-070-17646-44965BX.svs	HTA3_0044_1300965	HTA3_0044_1900965
PCGA-01-0044-070-17898-01130BX.svs	HTA3_0044_1301130	HTA3_0044_1901130
PCGA-01-0044-089-17646-44966BX.svs	HTA3_0044_1300966	HTA3_0044_1900966
PCGA-01-0044-089-17898-01131BX.svs	HTA3_0044_1301131	HTA3_0044_1901131
PCGA-01-0044-089-18295-01396BX.svs	HTA3_0044_1301396	HTA3_0044_1901396
PCGA-01-0045-045-17021-00893BX.svs	HTA3_0045_1300893	HTA3_0045_1900893
PCGA-01-0045-048-17021-00894BX.svs	HTA3_0045_1300894	HTA3_0045_1900894

PCGA-01-0045-048-17497-01241BX.svs	HTA3_0045_1301241	HTA3_0045_1901241
PCGA-01-0045-085-17021-00891BX.svs	HTA3_0045_1300891	HTA3_0045_1900891
PCGA-01-0045-085-17497-01238BX.svs	HTA3_0045_1301238	HTA3_0045_1901238
PCGA-01-0046-047-26739-00766BX.svs	HTA3_0046_1300766	HTA3_0046_1900766
PCGA-01-0046-047-27551-01292BX.svs	HTA3_0046_1301292	HTA3_0046_1901292
PCGA-01-0046-050-27138-00953BX.svs	HTA3_0046_1300953	HTA3_0046_1900953
PCGA-01-0046-050-27551-01293BX.svs	HTA3_0046_1301293	HTA3_0046_1901293
PCGA-01-0046-089-26739-00765BX.svs	HTA3_0046_1300765	HTA3_0046_1900765
PCGA-01-0046-089-27138-00952BX.svs	HTA3_0046_1300952	HTA3_0046_1900952
PCGA-01-0047-037-19263-01021BX.svs	HTA3_0047_1301021	HTA3_0047_1901021
PCGA-01-0047-037-19447-01216BX.svs	HTA3_0047_1301216	HTA3_0047_1901216
PCGA-01-0047-037-19809-01411BX.svs	HTA3_0047_1301411	HTA3_0047_1901411
PCGA-01-0047-050-19263-01022BX.svs	HTA3_0047_1301022	HTA3_0047_1901022
PCGA-01-0048-025-25305-48965BX.svs	HTA3_0048_1300965	HTA3_0048_1900965
PCGA-01-0048-025-25669-01275BX.svs	HTA3_0048_1301275	HTA3_0048_1901275

PCGA-01-0048-061-25669-01273BX.svs	HTA3_0048_1301273	HTA3_0048_1901273
PCGA-01-0048-061-25835-01381BX.svs	HTA3_0048_1301381	HTA3_0048_1901381
PCGA-01-0048-093-25102-00882BX.svs	HTA3_0048_1300882	HTA3_0048_1900882
PCGA-01-0048-093-25835-01380BX.svs	HTA3_0048_1301380	HTA3_0048_1901380
PCGA-01-0049-010-23043-01187BX.svs	HTA3_0049_1301187	HTA3_0049_1901187
PCGA-01-0050-050-23482-00998BX.svs	HTA3_0050_1300998	HTA3_0050_1900998
PCGA-01-0050-050-23699-01235BX.svs	HTA3_0050_1301235	HTA3_0050_1901235
PCGA-01-0050-084-23482-00997BX.svs	HTA3_0050_1300997	HTA3_0050_1900997
PCGA-01-0051-089-22577-01162BX.svs	HTA3_0051_1301162	HTA3_0051_1901162
PCGA-01-0051-089-22786-01334BX.svs	HTA3_0051_1301334	HTA3_0051_1901334
PCGA-01-0052-036-20842-01018BX.svs	HTA3_0052_1301018	HTA3_0052_1901018
PCGA-01-0052-036-21157-01301BX.svs	HTA3_0052_1301301	HTA3_0052_1901301
PCGA-01-0052-048-20842-01017BX.svs	HTA3_0052_1301017	HTA3_0052_1901017
PCGA-01-0052-048-21157-01302BX.svs	HTA3_0052_1301302	HTA3_0052_1901302
PCGA-01-0052-050-20842-01015BX.svs	HTA3_0052_1301015	HTA3_0052_1901015

PCGA-01-0052-093-20842-01014BX.svs	HTA3_0052_1301014	HTA3_0052_1901014
PCGA-01-0052-093-21157-01299BX.svs	HTA3_0052_1301299	HTA3_0052_1901299

Supplementary Table 1: HTAN IDs for the WSIs.